

Interaction of Spinons with Magnetic Fields in a Fractionalized State

Yu Zhang¹, Hengdi Zhao¹, Tristan R. Cao¹, Rahul Nandkishore^{1,2}, Pedro Schlottmann³,
Lance De Long⁴, and Gang Cao^{1,5*}

¹*Department of Physics, University of Colorado at Boulder, Boulder, CO 80309, USA*

²*Center for Theory of Quantum Matter, University of Colorado at Boulder, Boulder, CO 80309, USA*

³*Department of Physics, Florida State University, Tallahassee, FL 32306, USA*

⁴*Department of Physics and Astronomy, University of Kentucky, Lexington, KY 40506, USA*

⁵*Center for Experiments on Quantum Materials, University of Colorado at Boulder, Boulder, CO 80309, USA*

The 4d-electron trimer lattice $\text{Ba}_4\text{Nb}_{1-x}\text{Ru}_{3+x}\text{O}_{12}$ is believed to feature a universal heavy spinon Fermi surface that underpins both a quantum spin liquid (QSL) and an adjacent heavy-fermion strange metal (HFSM) phase, depending on Nb content. The itinerant spinons act as heat carriers that render the charge-insulating QSL a much better thermal conductor than the HFSM [1]. We find that application of magnetic field up to 14 T surprisingly induces an abrupt rise in the heat capacity by as much as 5000%, which breaks the signature linear temperature dependence of the heat capacity of both phases below 150 mK. In contrast, the AC magnetic susceptibility and the electrical resistivity show little response up to 14 T over the same milli-Kelvin temperature range. Applied magnetic field also readily suppresses the thermal conductivity by up to 40% with decreasing temperature below 4 K. All these complex thermal phenomena reveal that application of magnetic field drastically alters the behavior of spinons at low temperatures. The astonishing rise in the heat capacity (and thus entropy) at milli-Kelvin temperatures and strong magnetic fields presents a highly unusual situation that demands novel physics.

*Corresponding author: gang.cao@colorado.edu

Recent experimental works indicates that the trimer lattice $\text{Ba}_4\text{Nb}_{1-x}\text{Ru}_{3+x}\text{O}_{12}$ ($|x| < 0.20$) presents quantum spin liquid (QSL) physics, strong electron correlations tunable across a metal-to-insulator transition, and a heavy-fermion strange metal (HFSM) phase, as illustrated in **Fig.1a** [1]. The most striking feature shared by the entire $\text{Ba}_4\text{Nb}_{1-x}\text{Ru}_{3+x}\text{O}_{12}$ series is the ***persistent linearity*** of the low-temperature heat capacity C and thermal conductivity κ . These curious behaviors are accompanied by an extraordinarily large Sommerfeld coefficient γ and exchange energy θ_{cw} as well as the ***absence of magnetic order down to 50 mK***, independent of the ground state type (**Fig1.a**). Moreover, the charge-insulating QSL is a much better thermal conductor than the HFSM, and this is best explained by ***a charge and spin separation*** [1]. The key to the extraordinary behavior of this trimer lattice is a conjectured robust heavy Fermi surface of charge-neutral spinons that provides a unified framework for describing the novel phenomena observed throughout the entire series [1]. The discovery constitutes a breakthrough in the search of QSL that has been a focus of intense research over decades because of exotic excitations [e.g., 2-11].

Our most recent investigation of the trimer lattice $\text{Ba}_4\text{Nb}_{1-x}\text{Ru}_{3+x}\text{O}_{12}$ ($|x| < 0.20$; the sign of x can be either positive or negative) reveals an enigmatic, yet intriguing relationship between spinons and applied magnetic fields at low temperatures T , which has not yet been explored. In essence, applied magnetic field H (up to 14 T) unexpectedly breaks the signature linearity of the heat capacity C by inducing an abrupt rise in C near an onset temperature $T_s = 150$ mK for both the QSL and HFSM. Consequently, C is strongly increased by as much as 5000% at 50 mK. ***The field-enhanced change in C (ΔC) is remarkably independent of the orientation of H , indicating the absence of orbital degrees of freedom, consistent with the nature of spinons.*** Furthermore, no corresponding anomalies are discerned in both the AC magnetic susceptibility χ' of the QSL and HFSM or the electrical resistivity ρ of the HFSM under the same conditions. This work also

shows that application of H drastically reduces the thermal conductivity κ (particularly below 4 K) by as much as 40% for both the QSL and HFSM, but causes no discernible change in C , and therefore the density of states in the same T range ($1.7 < T < 10$ K). In short, application of H leads to an exotic quantum state featuring the abrupt rise in C at the most unlikely conditions of $T < 150$ mK and $\mu_0 H = 14$ T. *We argue that this emergent quantum state may be a result of field-induced localization of spinons when T approaches absolute zero.*

The $\text{Ba}_4\text{Nb}_{1-x}\text{Ru}_{3+x}\text{O}_{12}$ series forms in a trimer lattice that consists of three face-sharing metal-oxygen octahedra (**Fig.1a**) [1]. A trimer lattice often behaves unconventionally because the internal degrees of freedom between the three metal ions the trimer octahedra provide an extra, decisive interaction among other fundamental interactions (e.g., Coulomb and spin-orbit interactions) that dictates physical properties. It has become increasingly clear that heavy (high atomic number) trimer lattices promise a unique pathway for discoveries of new quantum states absent in materials with other types of lattices, such as triangular and perovskite lattices [1, 12-29]. The 4d-electron trimer lattice is a perfect example [1].

The trimer lattice adopts a rhombohedral structure with the R-3 space group (No. 148), in which a Nb-O monomer separates trimer layers along the c axis (**Fig.1a**) [1, 12, 30]. Depending on Nb concentration, the system exhibits both HFSM and adjacent QSL phases [1]. The former corresponds to $\text{Ba}_4\text{Nb}_{0.81}\text{Ru}_{3.19}\text{O}_{12}$ or $\text{Nb}_{0.81}$ and the latter $\text{Ba}_4\text{Nb}_{1.16}\text{Ru}_{2.84}\text{O}_{12}$ or $\text{Nb}_{1.16}$ (**Fig.1a**).

The exotic behavior of the heat capacity C is the central observation of this work. We first focus on C in the temperature range 50 mK – 1 K at $\mu_0 H = 0$ and 14 T for the HFSM and QSL (**Figs.1b-c**). As already established in our previous study [1], at $\mu_0 H = 0$ T, a linear C is persistent down to 50 mK with a large Sommerfeld coefficient $\gamma \leq 2650$ mJ/mole K² (**Figs.1b-c**). However, for $\mu_0 H = 14$ T, C rises rapidly below $T_s = 150$ mK for both the HFSM and QSL (**Figs.1b-c**). To

quantify the field-induced change of entropy, ΔS , we integrate $\Delta C = [C(14\text{T}) - C(0)]/T$ as $\Delta S = \int_{T_0}^{T_1} \frac{\Delta C}{T} dT$, where $T_0 = 0.05\text{ K}$ and $T_1 = 0.45\text{ K}$ for the QSL, as an example. The resulting ΔS , illustrated in **Fig. 1d**, reveals *a clear field-induced increases in entropy at lower temperatures*. ΔS below 0.2 K increases dramatically, reaching up to 0.22 J/mole K at 50 mK . This enhancement directly reflects the abrupt rise in C below $T_s \approx 150\text{ mK}$ (**Fig.1c**). Notably, C above T_s is essentially independent of magnetic field for both the QSL and HFSM phases (**Figs.1b-1c and 4d-4e**), suggesting that *the magnetic field produces a higher entropy state at low temperatures. The substantial low-temperature entropy release underscores the emergence of a large number of spinful, low-energy excitations induced by magnetic field — consistent with our proposed picture of localized spinon states forming effective two-level systems discussed below.*

Moreover, the field-induced increase in C , defined by $\Delta C/C(0) = [C(H) - C(0)]/C(0)$, can reach as high as 5000% at 50 mK (**Figs.2a-2b**), consistent with the enhancement in ΔS below T_s (**Fig.1d**). All these results strikingly contradict the conventional wisdom that a strong applied magnetic field (e.g., 14 T) coupled with low temperature (e.g., 50 mK) should generally strongly depress entropy by promoting order that reduces internal energy.

In sharp contrast with C (**Figs.1b-c**), both the a -axis resistivity ρ_a for the HFSM and AC magnetic susceptibility χ_a' for both the QSL and HFSM measured in the same temperature range display only a *featureless* response to 14 T (**Figs.2c-2d and Fig.S1**).

Notably, ΔC is independent of the orientation of H for both HFSM and QSL, as evidenced in $C(T)$ for $\mu_0 H = 14\text{ T}$ (**Figs.1b-1c**) and $C(H)$ at $T = 100\text{ mK}$ (**Fig. 2e**). The lack of the H -orientation dependence indicates *an absence of the orbital coupling* and an important role of the Zeeman interaction through which the relevant degrees of freedom couple to H , which further highlights the nature of spinons as fractional excitations.

In contrast, both ρ_a and ρ_c at higher temperatures (e.g, 5 K) for the QSL are a strong function of H-orientation, and exhibit a strong oscillatory behavior with as a function of the angle between H and the applied current I, *revealing a strong orbital dependence* (Fig.S2). The magneto-resistivity ratio, defined by $\Delta\rho/\rho(0) = [\rho(H)-\rho(0)]/\rho(0)$, can be as high as 60% at 9 T. It is remarkable that $\Delta\rho/\rho(0)$ is predominantly positive for the *a*-axis ρ_a and negative for the *c*-axis ρ_c (SFig.2). Such a giant, anisotropic oscillatory magnetoresistance suggests an orbital quantum interference in the variable range hopping regime [20 and references therein], which is interesting in its own right (note no long-range magnetic order down to 50 mK). Nevertheless, *the contrasting transport behavior further highlights the spin-charge separation in the system at low temperatures.*

For comparison and contrast, the heat capacity C of a related trimer metal, 9R-BaRuO₃, as well as insulating Nb₂O₅ is also measured as functions of T (Fig.1e) and H (Fig.2f) at the same experimental conditions. Both the T - and H -dependences of C exhibit no similarities to those of the HFSM and QSL (Figs.1b-1c and 2e), which decisively eliminates any possible spurious effects from the Ba, Ru, and Nb starting materials and/or contributions from the nuclear heat capacity of those elements. Therefore, *the observed ΔC anomalies must be unique to Ba₄Nb_{1-x}Ru_{3+x}O₁₂.*

Nevertheless, the field-induced upturn in C (Fig.1b-c) could be related to a possible Schottky-like effect due to a splitting of two-levels, δ ; it could thereby be a high- T tail of a Schottky peak located well below 50 mK, therefore experimentally inaccessible, but become visible because H broadens δ and shifts up the Schottky peak to higher T . As such, for $T \gg \delta$, the Schottky contribution to C is expectedly proportional to DT^{-2} (D = Schottky coefficient). Combining DT^{-2} with a γT contribution due to spinons yields a total $C = \gamma T + DT^{-2}$ that describes $C(T)$ for both phases over $50 \text{ mK} \leq T \leq 1 \text{ K}$ in the presence of a strong H . *Note that the phonon contribution to*

C ($\sim T^3$) is either zero or negligible as the observed C show a robust linear temperature dependence over $50 \text{ mK} \leq T \leq 8 \text{ K}$ at $H = 0$ (Fig.1b-1c and [1]). This is because the phonon contribution (positive β) is compensated by the second term of the Sommerfeld expansion of the electronic contribution (negative β) yielding a measured β that is essentially zero [1]. Fitting $C(T, 14\text{T})$ to $C/T = \gamma + DT^{-3}$ generates a linear fit that determines values of D for both phases at $\mu_0 H = 14 \text{ T}$ (Fig.3a). Additionally, $C(H)$ basically scales with H^2 below 200 mK (Fig.3b). A few features are worth noting: (1) The D values for both phases are essentially identical, *suggesting that the degrees of freedom responsible for ΔC are the same*; and (2) The magnitude of the D values, 10^{-3} JK/mole , is three orders of magnitude greater than 10^{-6} JK/mole due to the quadrupolar and/or magnetic spin splitting of Ru nuclei [32 and references therein], suggesting that the Schottky physics (if such it is) is *not of nuclear origin*.

For comparison, similar measurements are conducted for a 2.5% Pr doped isostructural $\text{Ba}_4\text{Nb}_{1-x}\text{Ru}_{3+x}\text{O}_{12}$ i.e., $\text{Ba}_{3.90}\text{Pr}_{0.10}\text{Nb}_{0.84}\text{Ru}_{3.16}\text{O}_{12}$, in which the Pr doping introduces a conventional Schottky anomaly characterized by an upturn in C at $H = 0$ below 200 mK (Fig.3e). This clear Schottky anomaly rapidly shifts to higher T with increasing H . In contrast, the upturn in C for both the HFSM and QSL is steeper and relatively less field-sensitive, as shown in Figs.3c-3d. Notably, the magnitude of the upturn in C increases with H .

All in all, the data in Fig. 3 suggest that a conventional Schottky effect alone does not provide an adequate explanation of the $\Delta C(H)$ data for $T < T_s = 150 \text{ mK}$.

We now turn to the data for the thermal conductivity κ over 1.7 K – 10 K at selected H . Our previous study has already established that the QSL is a much better thermal conductor than the HFSM and that both are dominated by spinons at low T [1]. What is equally intriguing is that application of a magnetic field readily suppresses κ in both phases (Figs.4a-4b). This is

inconsistent with experimental precedents [e.g., 33, 34, 35, 36, 37]; that is, generally, κ is proportional to C , the velocity v of heat carriers and the mean free path l of the heat carriers, i.e., $\kappa \sim Cvl$. Because v and l are essentially constant at low T [38], C is expected to dictate κ . Here, since C does not change with H in the same temperature range, 1.7 K – 10 K, as shown in **Fig.4d-4e**, *the observed reduction of κ indicates a significant reduction of the spinon velocity v due to H* . It cannot be ruled out the shortening of l of the spinons. As shown in **Fig.4a**, the magnetic field effect on the a -axis κ_a is strong initially when H increases from 0 T to 7 T but becomes weaker as H further increases from 7 T to 14 T, suggesting a trend for saturation with increasing H , which is consistent with the above argument.

Furthermore, a close examination of κ at selected H in **Fig.4a-4b** reveals that the magnetic-field effect on κ_a is a strong function of T below 4 K. Here, we introduce a magneto-thermal-conductivity ratio, defined by $\Delta\kappa_a/\kappa_a(0T) = [\kappa_a(14T) - \kappa_a(0T)]/\kappa_a(0T)$, to quantify the reduction in κ_a due to the applied 14 T. Note that $\Delta\kappa_a$ reflects contributions from heat carriers that are susceptible to H , i.e., H -reduced κ_a . Since the QSL is a charge insulator, $\Delta\kappa_a$ must be due primarily to spinons at low T . *It is important to point out that a phonon contribution to κ ($\sim T^3$) is unlikely below 8 K where both κ and C vary linearly with T (Figs 1b-1c, 4a-4b and [1]).* As shown in **Fig.4c**, $\Delta\kappa_a/\kappa_a(0T)$ as a function of T shows an unusually large reduction in κ_a . This reduction is considerably stronger in the QSL than in the HFSM (**Fig.4c**). Such a difference is consistent with there being more spinons as heat carriers in the QSL than in the HFSM (consistent also with the larger C and κ in the QSL [1]), which naturally makes the QSL a much better thermal conductor than the HFSM (**Fig.4a-4b**). Indeed, $\Delta C/C(0)$ is larger in the QSL than in the HFSM (**Fig.2a-2b**). These observations provide an additional, key testament to the crucial role of spinons in the

behavior of the trimer systems. Note that the spinons also dominate $C(T)$ and $\kappa(T)$ in the HFSM where the Wiedemann-Franz law is strongly violated, consistent with the spin-charge separation [1].

In addition, $\Delta\kappa_a/\kappa_a(0T)$ for both phases exhibits a rapid downturn at $T < 4$ K, resulting in a swift reduction in κ_a by as much as 40% near 1.7 K (**Fig.4c**). Because C in the same temperature range remains unchanged (**Figs.4d-4e**), the increasingly negative $\Delta\kappa_a/\kappa_a(0T)$ with decreasing T (**Fig.4c**) forcefully indicates that *it must be the mobility of spinons that decreases rapidly with decreasing T as a result of the applied magnetic field*. At this rate of the deceleration of spinons, it is conceivable that a strong magnetic field such as 14 T could eventually localize otherwise itinerant spinons when T approaches milli-Kelvin temperatures. This point is schematically illustrated in **Fig.4f**.

In short, the most striking experimental feature in this work is the dramatic upturn in $C(T)$, appearing below $T_s \approx 150$ mK under a magnetic field of 14 T (**Figs.1b-1c**). This anomaly is field-orientation independent and is not accompanied by corresponding features in either the magnetic susceptibility or electrical resistivity, ruling out conventional phase transitions (**Figs.2c-2d** and **SFig.1**). The scaling of $C(H) \propto H^2/T^2$ suggests a Schottky-like behavior, but with magnitudes far exceeding nuclear contributions (**Fig.3a-3b**). All these phenomena underscore an extraordinary susceptibility of itinerant spinons to applied magnetic fields at milli-Kelvin temperatures, which, however, has never been explored before, either experimentally or theoretically. (Notably, the strong linear temperature dependence of C , ρ , and κ at low temperatures effectively rules out impurity or chemical disorder as contributing factors to the observed novel phenomena.)

We propose that the dramatic low- T upturn in $C(T)$ arises from the *field-induced localization of spinons*, which are itinerant and charge-neutral excitations dominating

both C and κ in the QSL and HFSM. In the absence of magnetic field, the spinons are weakly antilocalized due to symplectic symmetry [39]. Application of a magnetic field breaks time-reversal symmetry and changes the symmetry class, suppressing antilocalization and enabling Anderson localization at low temperatures, as schematically shown in **Fig.4g**.

We conjecture that spinon localization gives rise to the emergence of spinful two-level systems (local moments) *whose Zeeman splitting produces the observed spinon Schottky anomaly in $C(T)$* (**Figs.1c-1d**). The simplest interpretation is that the local moments consist of individual, localized spinons. However, it is also possible that interactions between these spinons give rise to spin-glass ordering, with the emergent "two-level systems" representing dynamical droplets within a spin-glass state [40]. In either scenario, the formation of two-level systems results in a significant release of entropy, ΔS (up to 0.22 J/mol·K at 50 mK), as shown in **Fig. 1d**. This behavior may be consistent with a high density of weakly interacting localized states [e.g., 41, 42].

This interpretation is further supported by the thermal conductivity data: while C remains constant between 2–10 K (**Figs.4d-4e**), κ is strongly suppressed by field (**Figs.4a-4c**), implying a reduction in spinon mobility. The downturn in $\Delta\kappa/\kappa(0)$ below 4 K and its increasing suppression with field align naturally with the onset of spinon localization.

An alternative, more exotic explanation invokes fractional excitations with restricted mobility (fractons) which pair into mobile spinons in the absence of field [8, 43]. Under magnetic field, such composites could unbind into immobile constituents, but this scenario lacks a natural explanation for the sharp onset temperature T_s and thus appears less compelling than the localization scenario.

This work reveals a new, fundamental relationship between spinons and magnetic fields: As T approaches absolute zero, a strong magnetic field drastically changes the behavior of spinons,

leading to emergent phenomena in a quantum material dictated by spin-charge separation, which merits more investigations both experimentally and theoretically.

METHODS

Crystal Growth and Characterization

Single crystals of $\text{Ba}_4\text{Nb}_{1-x}\text{Ru}_{3+x}\text{O}_{12}$ ($|x| < 0.20$) were grown via a high-temperature flux method. Stoichiometric amounts of high-purity BaCO_3 , Nb_2O_5 , and RuO_2 powders were thoroughly mixed with an excess of BaCl_2 flux (mass ratio $\approx 1:3$). The mixture was loaded into an alumina crucible and heated to 1280°C for 38 hours. The melt was then slowly cooled to 800°C at a rate of $2^\circ\text{C}/\text{hour}$, followed by rapid quenching to room temperature.

The resulting single crystals of $\text{Ba}_4\text{Nb}_{1-x}\text{Ru}_{3+x}\text{O}_{12}$ were characterized using a Bruker Quest ECO single-crystal diffractometer with an Oxford Cryosystem providing sample temperature environments ranging from 80 K to 400 K. Chemical analyses of the samples were performed using a combination of a Hitachi MT3030 Plus scanning electron microscope and an Oxford Energy Dispersive X-Ray Spectrometer (EDX). The measurements of the electrical resistivity, Hall effect, heat capacity, thermal conductivity and AC magnetic susceptibility were carried out using a Quantum Design (QD) Dynacool PPMS system with a 14-Tesla magnet, a dilution refrigerator, a homemade probe for thermal conductivity, and a set of external meters that measure current and voltage with high precision.

The samples used in this study were from the same batches as those reported in Ref. [1], with additional crystals grown for reproducibility checks. All heat capacity and thermal conductivity results shown here were confirmed on at least two independently prepared crystals per composition.

Supplemental Remarks on AC Susceptibility and resistivity at the milli-Kelvin range

For completeness, we show the temperature dependence of the AC magnetic susceptibility of the HFSM in the mK range as **Supplemental SFig.1**. As expected, it shows featureless responses under field, consistent with our assertion that the low-temperature heat capacity anomaly is not reflected in charge or magnetic transport channels.

The QSL becomes very insulating at low temperatures, and the resistivity reaches up to 10^5 Ω -cm near 5 K (see Fig.1 in Ref.1). As such, resistivity measurements of the QSL in the mK range becomes impossible because all electronics will be out of range.

Supplemental Remarks on Magnetoresistance

Both a-axis and c-axis electrical resistivity ρ_a and ρ_c at higher temperatures for the quantum spin liquid (QSL) are a strong function of H-orientation, exhibiting a strong oscillatory behavior with the angle between H and the applied current I (**Supplemental SFig. 2**). The magnetoresistivity ratio, defined by $\Delta\rho/\rho(0) = [\rho(H) - \rho(0)]/\rho(0)$, can be as high as 60% at 9 T. Remarkably, $\Delta\rho/\rho(0)$ is positive for the *a*-axis ρ_a and negative for the *c*-axis ρ_c (**SFig. 1**). This suggests strong layer-like structure, and is also consistent with earlier observations that inter and intra-layer transport are dominated by different carriers. In short, such a giant, anisotropic oscillatory magnetoresistance suggests an orbital quantum interference in the variable range hopping regime, which is interesting in its own right (Note no magnetic order down to 50 mK). Nevertheless, the contrasting transport behavior further highlights the spin-charge separation in the system, that is, the heat capacity and thermal conductivity are dominated by different degrees of freedom to those which control charge transport.

DATA AVAILABILITY

The data that support the findings of this work are available from the corresponding authors upon request.

REFERENCES

1. Hengdi Zhao, Yu Zhang, Pedro Schlottmann, Lance DeLong, Rahul Nandkishore and Gang Cao, Transition between heavy-fermion-strange-metal and spin liquid in a 4d-electron trimer lattice, *Phys. Rev. Lett.* **132**, 226503 (2024)
2. P. W. Anderson, Resonating valence bonds: a new kind of insulator? *Mater. Res. Bull.* **8**, 153–160 (1973)
3. P.W. Anderson, The resonating valence bond state in La_2CuO_4 and superconductivity, *Science* **235**, 1196 (1987)
4. P. A. Lee, An End to the Drought of Quantum Spin Liquids, *Science* **321**, 1306-1307 (2008)
5. L. Savary, L. Balents, Quantum spin liquids: A review, *Rep. Prog. Phys.* **80**, 016502 (2017).
6. Y. Zhou, K. Kanoda, T.-K. Ng, Quantum spin liquid states, *Rev. Mod. Phys.* **89**, 025003 (2017).
7. C. Broholm, R. Cava, S. Kivelson, D. Nocera, M. Norman, T. Senthil, Quantum spin liquids, *Science* **367**, 263 (2020)
8. Rahul M. Nandkishore and Michael Hermele, Fractons, *Annu. Rev. Condens. Matter Phys.* **10**, 295 (2019)
9. Banerjee, S., Zhu, W. & Lin, SZ. Electromagnetic signatures of a chiral quantum spin liquid. *npj Quantum Mater.* **8**, 63 (2023)
10. Hong, X., Gillig, M., Yao, W. *et al.* Phonon thermal transport shaped by strong spin-phonon scattering in a Kitaev material $\text{Na}_2\text{Co}_2\text{TeO}_6$. *npj Quantum Mater.* **9**, 18 (2024)
11. Razpopov, A., Kaib, D.A.S., Backes, S. *et al.* A $j_{\text{eff}} = 1/2$ Kitaev material on the triangular lattice: the case of NaRuO_2 . *npj Quantum Mater.* **8**, 36 (2023)

12. L. T. Nguyen, T. Halloran, W. Xie, T. Kong, C. L. Broholm, and R. J. Cava, Geometrically frustrated trimer-based Mott insulator, *Phys. Rev. Mater.* **2**, 054414 (2018)
13. L. T. Nguyen and R. J. Cava, Trimer-based spin liquid candidate $\text{Ba}_4\text{NbIr}_3\text{O}_{12}$, *Phys. Rev. Materials* **3**, 014412 (2019).
14. L. T. Nguyen and R. J. Cava, Hexagonal Perovskites as Quantum Materials, *Chem. Rev.* **121**, 2935 (2021)
15. S. V. Streltsov and D. I. Khomskii, Cluster Magnetism of $\text{Ba}_4\text{NbMn}_3\text{O}_{12}$: Localized Electrons or Molecular Orbitals, *JETP Lett.* **108**, 686 (2018).
16. Evgenia V. Komleva, Daniel I. Khomskii, and Sergey V. Streltsov, Three-site transition-metal clusters: Going from localized electrons to molecular orbitals, *Phys. Rev. B* **102**, 174448 (2020)
17. G. Cao, H. D. Zhao, H. Zheng, Y. F. Ni, Christopher. A. Pocs, Y. Zhang, Feng, Ye, Christina Hoffmann, Xiaoping Wang, Minhyea Lee, Michael Hermele and Itamar Kimchi, Quantum liquid from strange frustration in the trimer magnet $\text{Ba}_4\text{Ir}_3\text{O}_{10}$, *npj Quantum Materials* **5**, 26 (2020)
18. Y. Shen, J. Sears, G. Fabbris, A. Weichselbaum, W. Yin, H. Zhao, D. G. Mazzone, H. Miao, M. H. Upton, D. Casa, R. S. Acevedo-Esteves, C. Nelson, A. M. Barbour, C. Mazzoli, G. Cao, and M. P. M. Dean, Emergence of spinons in layered trimer iridate $\text{Ba}_4\text{Ir}_3\text{O}_{10}$, *Phys. Rev. Lett.* **129**, 207201 (2022)
19. A. Sokolik, S. Hakani, S. Roy Susmita, N. Pellatz, H. Zhao, G. Cao, I. Kimchi, D. Reznik, Spinons and damped phonons in spin-1/2 quantum-liquid $\text{Ba}_4\text{Ir}_3\text{O}_{10}$ observed by Raman scattering, *Phys. Rev. B* **106**, 075108 (2022)

20. Yu Zhang, Yifei Ni, Hengdi Zhao, Sami Hakani, Feng Ye, Lance DeLong, Itamar Kimchi, and Gang Cao, Control of chiral orbital currents in a colossal magnetoresistance material, *Nature* **611**, 467 (2022)
21. Yu Zhang, Yifei Ni, Pedro Schlottmann, Rahul Nandkishore, Lance DeLong and Gang Cao, Current-sensitive Hall effect in a chiral-orbital-current state. *Nat Commun* **15**, 3579 (2024)
22. I. Terasaki, S. Ito, T. Igarashi, S. Asai, H. Taniguchi, R. Okazaki, Y. Yasui, K. Kobayashi, R. Kumai, H. Nakao, and Y. Murakami, Novel charge ordering in the trimer iridium oxide BaIrO_3 , *Crystals* **6**, 27 (2016)
23. R. Okazaki, S. Ito, K. Tanabe, H. Taniguchi, Y. Ikemoto, T. Moriwaki, and I. Terasaki, Spectroscopic signature of trimer Mott insulator and charge disproportionation in BaIrO_3 , *Phys. Rev. B* **98**, 205131 (2018)
24. M. Ye, H.-S. Kim, J.-W. Kim, C.-J. Won, K. Haule, D. Vanderbilt, S.-W. Cheong, and G. Blumberg, Covalency-driven collapse of strong spin-orbit coupling in face-sharing iridium octahedra, *Phys. Rev. B* **98**, 201105(R) (2018)
25. Y. Wang, R. Wang, J. Kim, M. H. Upton, D. Casa, T. Gog, G. Cao, G. Kotliar, M. P. M. Dean, and X. Liu, Direct Detection of Dimer Orbitals in $\text{Ba}_5\text{AlIr}_2\text{O}_{11}$, *Phys. Rev. Lett.* **122**, 106401 (2019)
26. Y. Klein, G. Rousse, F. Damay, F. Porcher, G. Andre, and I. Terasaki, Antiferromagnetic order and consequences on the transport properties of $\text{Ba}_4\text{Ru}_3\text{O}_{10}$, *Phys. Rev. B* **84**, 054439 (2011)

27. S. V. Streltsov and D. I. Khomskii, Unconventional magnetism as a consequence of the charge disproportionation and the molecular orbital formation in $\text{Ba}_4\text{Ru}_3\text{O}_{10}$, *Phys. Rev. B* **86**, 064429 (2012)
28. T. Igarashi, R. Okazaki, H. Taniguchi, Y. Yasui, and I. Terasaki, Effects of the Ir impurity on the thermodynamic and transport properties of $\text{Ba}_4\text{Ru}_3\text{O}_{10}$, *J. Phys. Soc. Jpn.* **84**, 094601 (2015)
29. J. Sannigrahi, A. Paul, A. Banerjee, D. Khalyavin, A. D. Hillier, K. Yokoyama, A. K. Bera, M. R. Lees, I. Dasgupta, S. Majumdar, and D. T. Adroja, Orbital effects and Affleck Haldane-type spin dimerization in $\text{Ba}_4\text{Ru}_3\text{O}_{10}$, *Phys. Rev. B* **103**, 144431 (2021)
30. Supplemental Material
31. L. B. Ioffe, B. Z. Spivak, Giant magnetoresistance in the variable-range hopping regime. *J. Exp. Theor. Phys.* **117**, 551–569 (2013)
32. Z. X. Zhou, S. McCall, C.S. Alexander, J.E. Crow, P. Schlottmann, A. Bianchi, C. Capan, R. Movshovich, K.H. Kim, M. Jaime, and N. Harrison, M. Haas, R. Cava and G. Cao, Transport and thermodynamic properties of $\text{Sr}_3\text{Ru}_2\text{O}_7$ near the quantum critical point, *Phys. Rev. B* **69**, 140409 (2004)
33. Ian A. Leahy, Christopher A. Pocs, Peter E. Siegfried, David Graf, S.-H. Do, Kwang-Yong Choi, B. Normand, and Minhyea Lee, Anomalous Thermal Conductivity and Magnetic Torque Response in the Honeycomb Magnet $\alpha\text{-RuCl}_3$, *Phys. Rev. Lett.* **118**, 187203 (2017)
34. P. Czajka, T. Gao, M. Hirschberger, *et al.* Oscillations of the thermal conductivity in the spin-liquid state of $\alpha\text{-RuCl}_3$. *Nat. Phys.* **17**, 915–919 (2021)
35. J F Gregg and D ter Haar, On the effect of a magnetic field on the thermal conductivity, *Eur. J. Phys.* **17** 303 (1996)

36. Rajasree Das, Amit Chanda and Ramanathan Mahendiran, Influence of magnetic field on electrical and thermal transport in the hole doped ferromagnetic manganite: $\text{La}_{0.9}\text{Na}_{0.1}\text{MnO}_3$, *RSC Adv.* **9**, 1726 (2019)
37. N. Wakeham, A. Bangura, X. Xu, *et al.* Gross violation of the Wiedemann–Franz law in a quasi-one-dimensional conductor. *Nat Commun* **2**, 396 (2011)
38. F. Steckel, A. Matsumoto, T. Takayama, H. Takagi, B. Buchner and C. Hess, Pseudospin transport in the $J_{\text{eff}} = 1/2$ antiferromagnet Sr_2IrO_4 , *EPL* **114** 57007 (2016)
39. S. Hikami, A.I. Larkin and Y. Nagaoka, Spin-orbit interaction and magnetoresistance in the two dimensional random system, *Progress of Theoretical Physics* 63, 2, 707 (1980)
40. Daniel S. Fisher and David A. Huse, Equilibrium behavior of the spin-glass ordered phase. *Phys. Rev. B* **38**, 386 (1988)
41. Lu Liu, Hui Shao, Yu-Cheng Lin, Wenan Guo, and Anders W. Sandvik. Random-Singlet Phase in Disordered Two-Dimensional Quantum Magnets. *Phys. Rev. X* **8**, 041040 (2018)
42. Itamar Kimchi, Adam Nahum, and T. Senthil. Valence Bonds in Random Quantum Magnets: Theory and Application to YbMgGaO_4 . *Phys. Rev. X* **8**, 031028 (2018)
43. A. Gromov and L. Radzihovsky, *Colloquium: Fracton matter*, *Rev. Mod. Phys.* 96, 011001 (2024)

ACKNOWLEDGEMENTS G.C. thanks Xi Dai, Tai-Kai Ng, Feng Ye, Sandeep Sharma, Minhyea Lee and Longji Cui for useful discussions. Experimental work is supported by National Science Foundation via Grant No. DMR 2204811. Theoretical work by R.N. was supported by the U.S. Department of Energy (DOE), Office of Science, Basic Energy Sciences (BES) under Award # DE-SC0021346.

AUTHOR CONTRIBUTIONS

Y.Z. conducted measurements of the physical properties; H.D.Z characterized the crystal structure of the crystals and conducted measurements of the physical properties. T.R.C. grew the single crystals and conducted measurements of the physical properties. R.N. conducted the theoretical analysis and contributed to paper revisions; P.S. conducted the theoretical analysis and contributed to paper revisions; L.D. contributed to paper revisions. G.C. initiated and directed this work, grew the single crystals, conducted experiments of physical properties, analyzed the data, constructed the figures, and wrote the paper.

COMPETING INTERESTS

The authors declare no competing interests.

FIGURE LENGENDS

Fig. 1. Key thermodynamic response of the trimer lattice $\text{Ba}_4\text{Nb}_{1-x}\text{Ru}_{3+x}\text{O}_{12}$. **a**, Schematic phase diagram as a function of Nb content x , illustrating the heavy spinon Fermi surface underpinning both the HFSM and QSL phases. The extraordinarily large Sommerfeld coefficient γ (blue) and exchange energy θ_{cw} (red, right scale) are shown [1]. Inset: The crystal structure of the trimer lattice. Note that the heavy-fermion strange metal (HFSM, $1-x = 0.81$ or $\text{Nb}_{0.81}$) and the insulating quantum spin liquid (QSL, $1-x = 1.16$ or $\text{Nb}_{1.16}$) are adjacent to each other. **b-c**, Heat capacity $C(T)$ for the HFSM and QSL, respectively, at 0 T and 14 T for both field orientations and for $50 \text{ mK} \leq T \leq 1 \text{ K}$. The black arrows mark the onset of the upturn in C , T_s . **d**, Temperature dependence of the entropy change ΔS obtained by integrating $\Delta C/T$ for the QSL. The significant enhancement of ΔS below 0.2 K is consistent with the strong upturn in C . **e**, Comparison with 9R-BaRuO_3 and Nb_2O_5 shows no upturn in C , confirming the intrinsic nature of the effect in $\text{Ba}_4\text{Nb}_{1-x}\text{Ru}_{3+x}\text{O}_{12}$.

Fig. 2. Contrasting responses in thermodynamic and transport properties. **a-b**, Relative change in heat capacity $[C(H) - C(0)]/C(0)$ vs. H for the QSL and HFSM, respectively, showing up to 5000% enhancement at 50 mK under 14 T. Note that the QSL shows a stronger change. **c-d**, Temperature dependence of the a -axis ρ_a for HFSM and the a -axis AC susceptibility χ'_a for the QSL at representative H , respectively, for $50 \text{ mK} \leq T \leq 1 \text{ K}$. **e**, The field dependence of C at $T =$

100 mK for the QSL at both $H \parallel a$ axis and $H \parallel c$ axis, confirming spinon Zeeman coupling without orbital contribution. **f**, No anomaly is observed in BaRuO_3 under similar conditions, further excluding a conventional nuclear or elemental origin.

Fig. 3. Analysis of the low-temperature heat capacity anomaly. **a**, C/T vs. $1/T^3$ for $50 \text{ mK} \leq T \leq 1 \text{ K}$ for both the HFSM and QSL. Note the slope D ($\sim 10^{-3} \text{ JK/mole}$) for both phases is essentially the same, and three orders of magnitude larger than that due to nuclear contributions. **b**, C as a function of H^2 at representative T for the QSL. **c–d**, Upturns in C for the HFSM and QSL grow in magnitude with field but share a common onset near $T_S = 150 \text{ mK}$. **e**, In contrast, Pr-doped $\text{Ba}_4\text{Nb}_{1-x}\text{Ru}_{3+x}\text{O}_{12}$ exhibits a conventional Schottky anomaly with stronger field sensitivity, highlighting the distinct mechanism in the undoped system.

Fig. 4. Thermal conductivity κ and spinon dynamics under magnetic fields. **a–b**, The a -axis thermal conductivity κ_a for the QSL and HFSM under various magnetic fields. **c**, The magneto-thermal-conductivity ratio $\Delta\kappa_a/\kappa_a(0T)$ as a function of T for the QSL and HFSM where $\Delta\kappa_a = \kappa_a(14T) - \kappa_a(0T)$. Note $\Delta\kappa_a/\kappa_a(0T)$ shows up to 40% suppression near 1.7 K. **d–e**, $C(T)$ over the same T range at $\mu_0H = 0$ and 14 T for the QSL and HFSM, respectively. Note that $C(T)$ remains essentially unchanged at 14 T. **f**, Schematic: Magnetic field reduces spinon velocity v at higher T and induces localization below T_S . **g**, Proposed T - H phase diagram for spinon dynamics, indicating a crossover from itinerant to localized behavior.

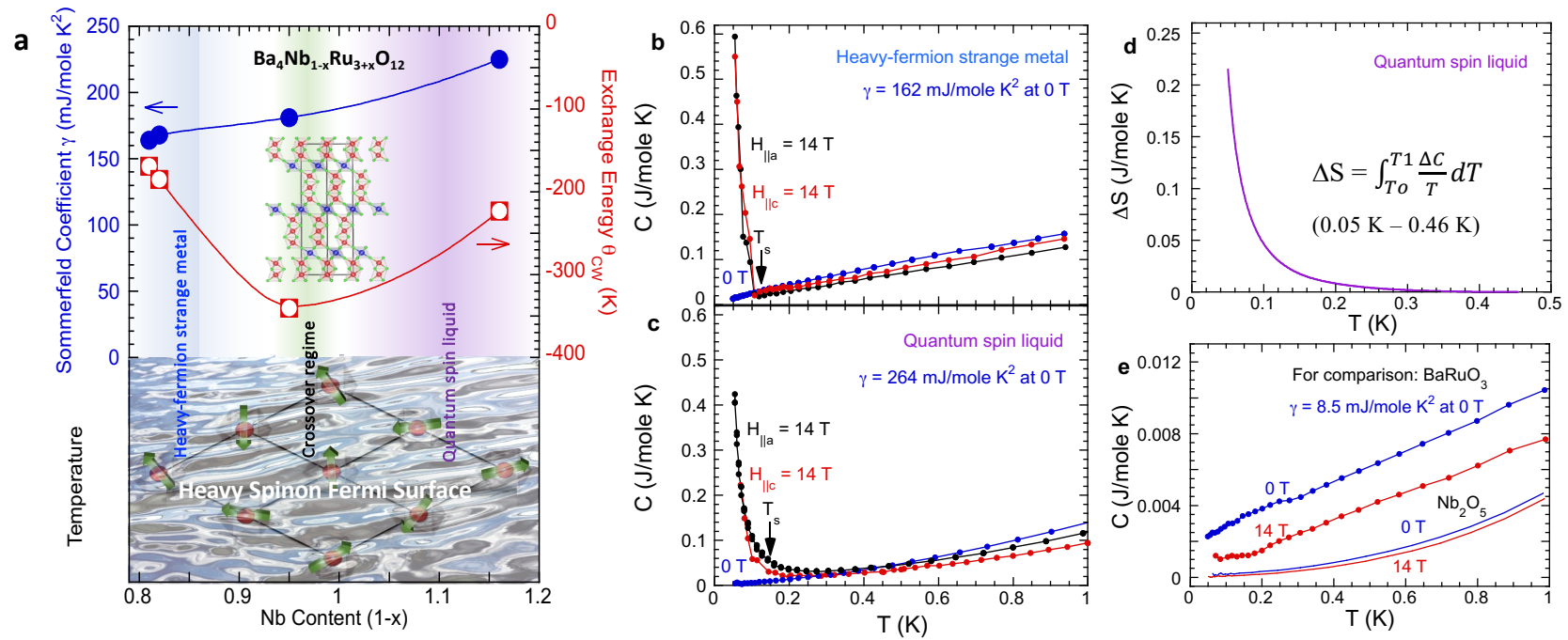


Figure 1

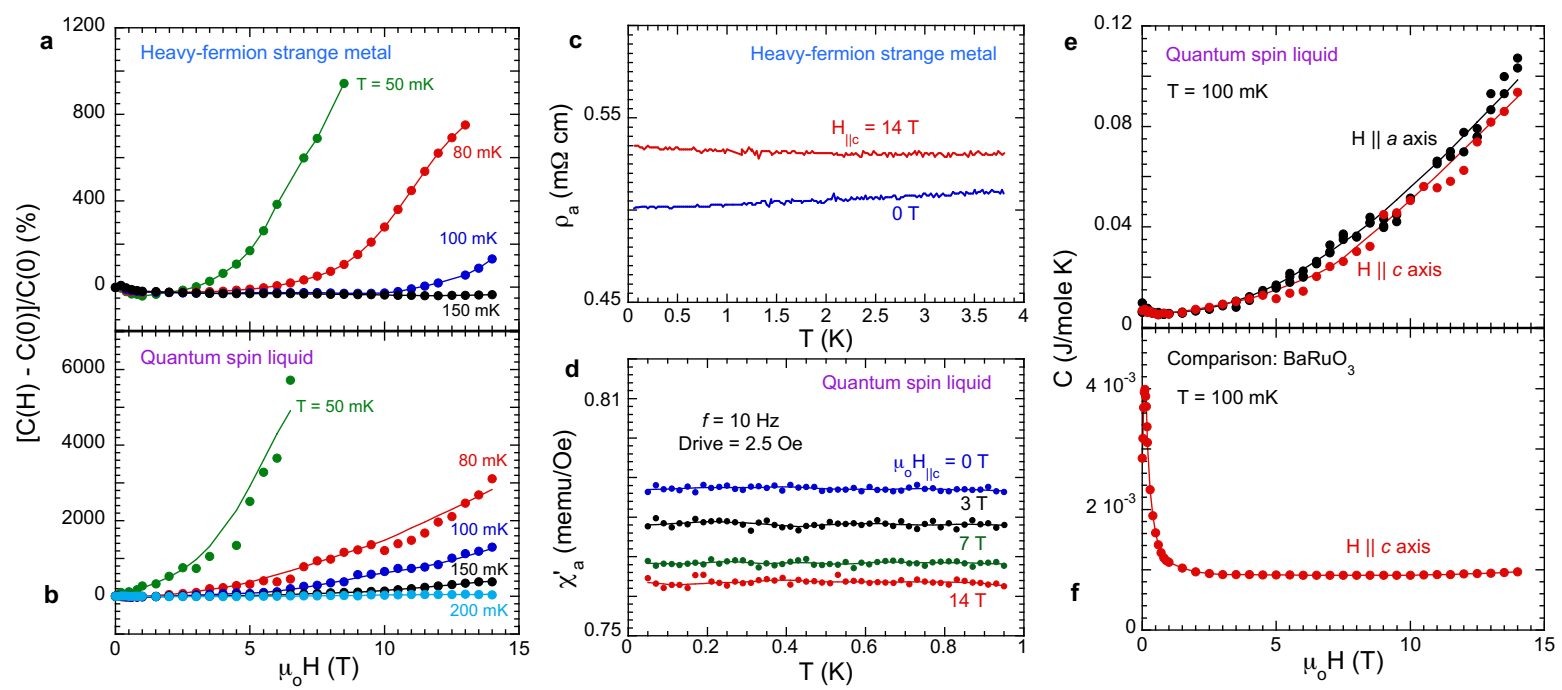


Figure 2

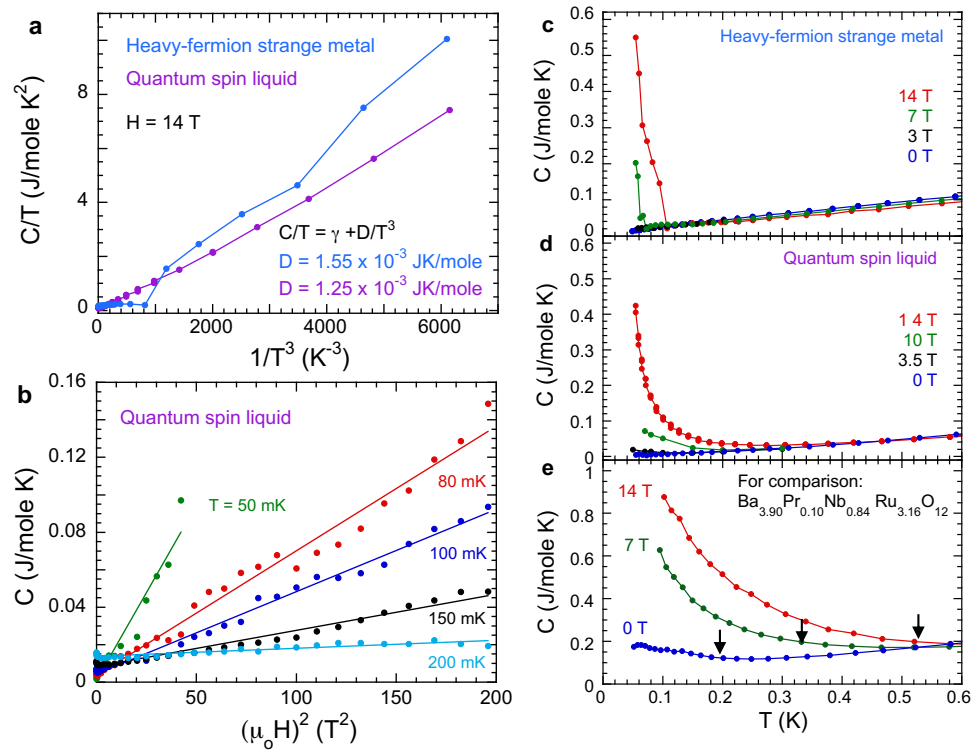


Figure 3

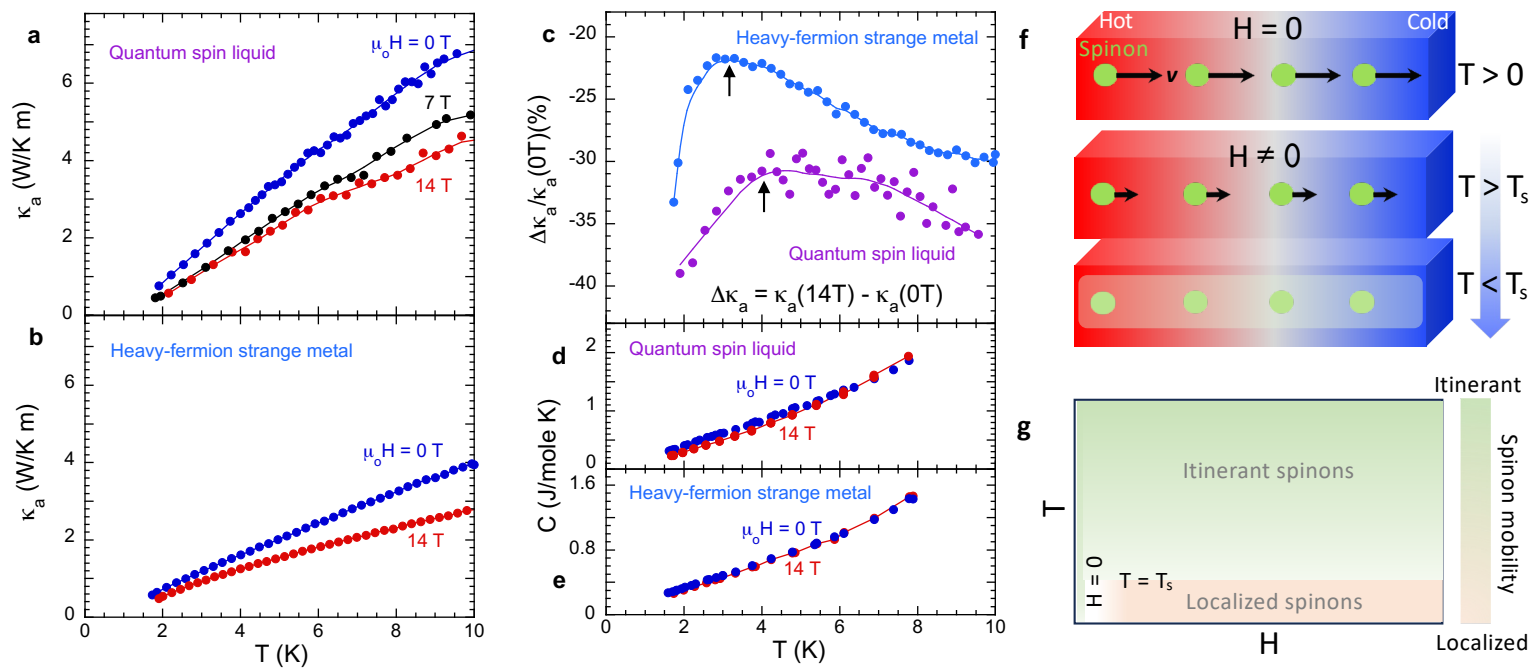


Figure 4